



## Short communication

Facile solution-based fabrication of  $\text{ZnIn}_2\text{S}_4$  nanocrystalline thin films and their photoelectrochemical propertiesYian Xie<sup>a</sup>, Yufeng Liu<sup>a,\*\*</sup>, Houlei Cui<sup>a</sup>, Wei Zhao<sup>a</sup>, Chongyin Yang<sup>a</sup>, Fuqiang Huang<sup>a,b,\*</sup><sup>a</sup> CAS Key Laboratory of Materials for Energy Conversion, Shanghai Institute of Ceramics, Chinese Academy of Sciences, Shanghai 200050, PR China<sup>b</sup> State Key Laboratory of Rare Earth Materials Chemistry and Applications, College of Chemistry and Molecular Engineering, Peking University, Beijing 100871, China

## H I G H L I G H T S

- Hexagonal  $\text{ZnIn}_2\text{S}_4$  nanocrystalline thin films are deposited by spin-coating method.
- $\text{ZnO}$  and  $\text{In}(\text{OH})_3$  are dissolved by thioacetic acid in precursor solution.
- $\text{ZnIn}_2\text{S}_4$  nanocrystals preferentially grow along c-axis *via* annealing in S vapor.
- $\text{ZnIn}_2\text{S}_4$  films show pronounced photoelectrochemical response under visible light.

## A R T I C L E I N F O

## Article history:

Received 10 January 2014

Received in revised form

26 February 2014

Accepted 17 March 2014

Available online 26 March 2014

## Keywords:

 $\text{ZnIn}_2\text{S}_4$  thin film

Solution method

Nanocrystal

Photoelectrochemical

## A B S T R A C T

Hexagonal phase  $\text{ZnIn}_2\text{S}_4$  nanocrystalline thin films are deposited by spin-coating method using an air-stable precursor solution. In the process, metal oxide and hydroxide are used as Zn and In sources to avoid the introduction of any anion impurity in  $\text{ZnIn}_2\text{S}_4$  thin films. The rod-like nanocrystalline grains with width and length about  $13 \pm 3$  nm and  $26 \pm 5$  nm grow along c-axis after annealing in sulfur vapor at 500 °C for 2 h. Smooth and compact thin films with different In/Zn ratios are fabricated by controlling the ratio of two metal sources in precursor solution. The flat-band potentials of these n-type  $\text{ZnIn}_2\text{S}_4$  thin films are in the range of  $-0.55$  to  $-0.45$  V vs. normal hydrogen electrode. The photoelectrochemical measurement demonstrates the excellent visible light response of  $\text{ZnIn}_2\text{S}_4$  thin films. The light current under visible light illumination occupies almost 60% of the light current under full spectrum illumination. The facile solution-based method provides a novel thought to fabricate high-quality thin films of multi metal chalcogenides with excellent photoelectric properties *via* solving the other metal oxide and hydroxide in the solution.

© 2014 Elsevier B.V. All rights reserved.

## 1. Introduction

As an important semiconductor material of ternary chalcogenides,  $\text{ZnIn}_2\text{S}_4$  has attracted lots of attention because of its considerable chemical stability, environmental benign and suitable band gap for visible light response [1]. Meanwhile,  $\text{ZnIn}_2\text{S}_4$  is the only member of  $\text{AB}_2\text{S}_4$  family semiconductors with a layer structure, and has great potential applications in charge storage [2], thermoelectricity [3], photocatalysis [4], hydrogen production [5], solar cell, [6]

photodetector [7] and so on. Various  $\text{ZnIn}_2\text{S}_4$  nanostructures and microstructures, for example, nanoplate [8], nanotube, nanoribbon [9], nanowire [10], submicrosphere [11], flower-like microsphere [12], have been successfully fabricated by numerous methods. Even so, fabrication of nanostructured  $\text{ZnIn}_2\text{S}_4$  thin films is still a great challenge, which limits their applications in thin film-based photoelectric devices. The reports on direct deposition  $\text{ZnIn}_2\text{S}_4$  thin films from physical and chemical methods are limited. The physical methods include single-source MOCVD [13], successive ionic layer adsorption and reaction (SILAR) technique [14] and magnetron sputtering [6], which are high-cost due to the use of expensive equipment. Deposition of  $\text{ZnIn}_2\text{S}_4$  thin films *via* chemical solution methods has got increasing attention in recent years.  $\text{ZnIn}_2\text{S}_4$  perpendicular nanosheet films are directly deposited on FTO substrates by a facile hydrothermal method [15]. Chemical bath

\* Corresponding author. CAS Key Laboratory of Materials for Energy Conversion, Shanghai Institute of Ceramics, Chinese Academy of Sciences, Shanghai 200050, PR China. Tel.: +86 21 52413214; fax: +86 21 52416360.

\*\* Corresponding author. Tel.: +86 21 52413214; fax: +86 21 52416360.

E-mail addresses: [liuyf@mail.sic.ac.cn](mailto:liuyf@mail.sic.ac.cn) (Y. Liu), [huangfq@mail.sic.ac.cn](mailto:huangfq@mail.sic.ac.cn) (F. Huang).

deposition (CBD) method is used to prepare Zn–In–S film electrodes [16] and Cu-doped  $\text{ZnIn}_2\text{S}_4$  films [17].  $\text{ZnIn}_2\text{S}_4$  film was fabricated on Ti substrate by a two-step approach including electrodeposition and annealing [18].

The special morphology and orientation of thin films play an important role in improving the photoelectric properties of thin film [19]. Otherwise, there are few investigations on  $\text{ZnIn}_2\text{S}_4$  thin films with special morphology and preferred growth. Herein, a non-vacuum solution-based method is presented to deposit hexagonal phase  $\text{ZnIn}_2\text{S}_4$  nanocrystalline thin films. Air-stable precursor solution is prepared by dissolution of ZnO and  $\text{In}(\text{OH})_3$  in thioacetic acid-based solution [20,21], avoiding the introduction of any anion impurity in  $\text{ZnIn}_2\text{S}_4$  thin films. The  $\text{ZnIn}_2\text{S}_4$  nanocrystals are formed and grow along c-axis *via* annealing in S vapor, resulting in the formation of well crystalline  $\text{ZnIn}_2\text{S}_4$  thin films. The element contents, crystal structure, morphology and optical properties of  $\text{ZnIn}_2\text{S}_4$  thin films with different In/Zn ratios are investigated. Furthermore, the  $\text{ZnIn}_2\text{S}_4$  thin films exhibit pronounced light current response under visible light illumination in photoelectrochemical measurement. The facile solution-based method provides a novel thought to fabricate high-quality thin films of multi metal chalcogenides with excellent photoelectric properties *via* solving the other metal oxide and hydroxide in the solution.

## 2. Experimental

### 2.1. Preparation of precursor solution

All chemicals were used as received without further purification. Precursor solutions with In/Zn ratios of 2, 2.5 and 3 were prepared. In a typical preparation of precursor solution, 0.5 mmol zinc (II) oxide ( $\text{ZnO}$ , analytical grade), 1 mmol, 1.25 mmol or 1.5 mmol indium (III) hydroxide ( $\text{In}(\text{OH})_3$ , 98%) (namely In/Zn = 2, 2.5 or 3) were added to a mixture solvent of 4 mL ethanol ( $\text{C}_2\text{H}_6\text{O}$ , analytical grade), 1 mL propylene glycol ( $\text{C}_3\text{H}_8\text{O}_2$ , analytical grade) and 2 mL thioacetic acid ( $\text{CH}_3\text{COSH}$ , 93%). After stirring for 5 min, ammonia was added into the white suspension under continuous stirring at room temperature until a light yellow, clear precursor solution was obtained.  $\text{ZnIn}_2\text{S}_4$  thin films deposited from different precursor solutions were labeled as ZIS-X (X = In/Zn ratio in precursor solution).

### 2.2. Deposition of $\text{ZnIn}_2\text{S}_4$ thin films

The  $\text{ZnIn}_2\text{S}_4$  thin films were deposited on fluorine-doped tin oxide (FTO) transparent conducting glass substrates *via* spin-coating method from the as-prepared precursor solution. Each layer was spin-coated with 1500 rpm for 20 s and subsequently dried on a 300 °C heating plate for 1 min to evaporate the organic solvents. The processes were repeated 6 times. Finally, the crystalline  $\text{ZnIn}_2\text{S}_4$  thin films were obtained through sulfuration in S vapor at 500 °C for 0.5–2 h.

### 2.3. Characterization

The In/Zn ratios in  $\text{ZnIn}_2\text{S}_4$  thin films were measured by electron probe microanalysis (EPMA JXA-8100) at an accelerating voltage of 20 kV. The crystallization and phase identification of the  $\text{ZnIn}_2\text{S}_4$  thin films were performed by X-ray diffraction (XRD Bruker D8 Focus) with a monochromatized source of  $\text{Cu K}\alpha 1$  radiation ( $\lambda = 0.15405$  nm) at 1.6 kW (40 kV, 40 mA). Raman spectra were collected on a Thermal Dispersive Spectrometer using a laser with an excitation wavelength of 532 nm at laser power of 10 mW. Low and high-resolution transmission electron microscopy (TEM) images were taken on a JEOL JEM-2100F at an accelerating voltage of

200 kV. Top-view and cross-sectional field emission scanning electron microscopy (FESEM) images were taken on JEOL JSM-6400F microscope. UV–Vis absorbance spectrums were recorded on a Hitachi U-3010 spectrophotometer with a scanning velocity of 300 nm  $\text{min}^{-1}$ . The electrochemical impedance measurements were performed in a typical three-electrode potentiostat system (Parstat 2773), in which the  $\text{ZnIn}_2\text{S}_4$  thin film on FTO substrate, a Pt wire and an Ag/AgCl electrode were used as the working, counter and reference electrodes, respectively. A 0.25 M  $\text{Na}_2\text{S}$  aqueous solution (pH = 13.5) was used as the supporting electrolyte to maintain the stability of films. Photoelectrochemical (PEC) measurements were performed in the same three-electrode potentiostat system. A solar simulator (AM 1.5) with a power of 100  $\text{mW cm}^{-2}$  was used as the illumination source. The visible light PEC response was measured under the same solar simulator cut off by a 400 nm filter. Photocurrent ON/OFF cycles were measured using the same electrochemical workstation coupled with a mechanical chopper.

## 3. Results and discussion

EPMA is performed to verify the In/Zn ratio in  $\text{ZnIn}_2\text{S}_4$  thin films. Fig. 1a shows the In/Zn ratios of ZIS-2.5 with different annealing times. The In/Zn ratio drops from 2.5 in precursor solution to 1.93 in thin film after depositing *via* spin-coating process. The loss of In may be caused by volatilization of In-organic species in precursor solution during the spin-coating process [22]. Then In/Zn ratios almost maintain around 1.95 after annealing for different times, indicating no loss of In during annealing process. The loss of In can be found in three samples after annealing for 2 h, as shown in Fig. 1b. The In/Zn ratios of annealed  $\text{ZnIn}_2\text{S}_4$  thin films are nearly linear with that of precursor solutions, implying the In/Zn ratios in  $\text{ZnIn}_2\text{S}_4$  thin films could be effectively adjusted by controlling the metal source components in precursor solution. So ZIS-2, ZIS-2.5 and ZIS-3 are In-poor, stoichiometric and Zn-poor  $\text{ZnIn}_2\text{S}_4$  thin films, respectively.

The phase and purity of  $\text{ZnIn}_2\text{S}_4$  thin films are determined by XRD. As shown in Fig. 2a, no characteristic peak of  $\text{ZnIn}_2\text{S}_4$  is observed in the XRD pattern of ZIS-2.5 raw film, indicating the amorphous phase before annealing. After annealing for 0.5 h, one weak and broad peak are observed at 21.9°, and the peak intensity enhances with annealing time increasing from 0.5 h to 2 h. In addition, another peak at 7.2° is found after annealing for 1 h. These two peaks at 7.2° and 21.9° can be indexed to the planes (002) and (006) of hexagonal phase of  $\text{ZnIn}_2\text{S}_4$  (JCPDS no. 72-0773). Of note, no other characteristic peak of hexagonal phase is observed even annealing for 2 h, which implies the preferred growth along c-axis of  $\text{ZnIn}_2\text{S}_4$  during annealing process. According to Scherrer formula ( $d = 0.89\lambda/B \cos \theta$ , where  $d$ ,  $\lambda$ ,  $B$ , and  $\theta$  are crystallite size,  $\text{Cu K}\alpha 1$

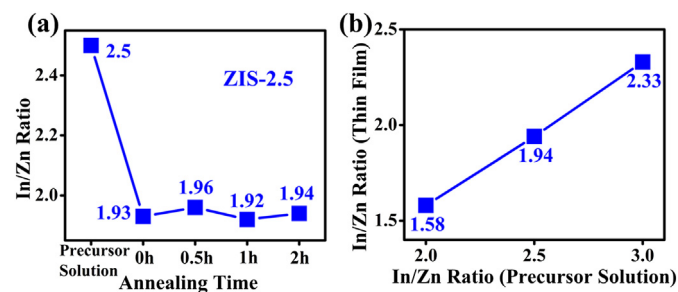
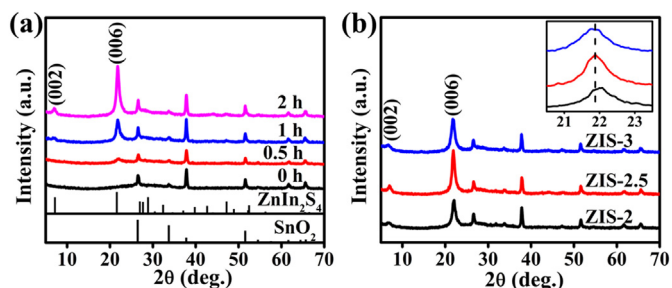


Fig. 1. (a) The In/Zn ratio of ZIS-2.5 with different annealing times and (b) In/Zn ratio in  $\text{ZnIn}_2\text{S}_4$  thin films after annealing for 2 h as a function of In/Zn ratio in precursor solutions.



**Fig. 2.** XRD patterns of (a) ZIS-2.5 with different annealing times and (b) ZnIn<sub>2</sub>S<sub>4</sub> thin films with different In/Zn ratios after annealing for 2 h. Inset shows the details of XRD patterns around 20.5° and 23.5° 2θ values. JCPDS files: ZnIn<sub>2</sub>S<sub>4</sub> (72-0773), SnO<sub>2</sub> (77-0452).

wavelength, full width at half-maximum intensity (FWHM) in radians and Bragg's diffraction angle, respectively), the nanocrystal-line size with annealing times of 0.5 h, 1 h and 2 h are calculated to be 12.5 nm, 14.5 nm and 14.7 nm, respectively. Otherwise, similar XRD patterns can be observed from ZnIn<sub>2</sub>S<sub>4</sub> thin films with different In/Zn ratios (Fig. 2b), demonstrating the preferred growth of the nanocrystal would not be hampered in Zn-poor or In-poor samples. The relatively low peak intensity of ZIS-2 and ZIS-3 comparing with ZIS-2.5 may be caused by lattice defect in Zn-poor or In-poor thin films. The diffraction peaks shift to lower theta value with the increase of In content because of the larger radius of In<sup>3+</sup> (0.81 Å) compared to that of Zn<sup>2+</sup> (0.74 Å), which also indicating that the metal ions were located at crystal lattice points.

Raman spectroscopy is used to obtain more information about the crystal structure of ZnIn<sub>2</sub>S<sub>4</sub> thin films. Fig. 3a shows the Raman spectra of ZIS-2.5 thin films with different annealing times. As for ZnIn<sub>2</sub>S<sub>4</sub> thin film before annealing, only one small peak around 355 cm<sup>-1</sup> is found. Three Raman peaks around 248, 308 and 355 cm<sup>-1</sup> in the spectra of annealed thin films are typical molecular vibration of ZnIn<sub>2</sub>S<sub>4</sub>, which can be assigned to the longitudinal optical mode (LO<sub>1</sub>), transverse optical mode (TO<sub>2</sub>) and longitudinal optical mode (LO<sub>2</sub>) of ZnIn<sub>2</sub>S<sub>4</sub> crystal, respectively [12,23]. The Raman spectra can further verify the formation of ZnIn<sub>2</sub>S<sub>4</sub> phase. As shown in Fig. 3b, the three peaks are also observed for ZIS-2 and ZIS-3 annealing for 2 h. However, the relatively low intensity of Raman peaks of ZIS-2 and ZIS-3 samples compared to that of ZIS-2.5 may be resulted from the lattice distortion caused by element stoichiometry deviation, which is agreed with the XRD results. No peak of impurity is detected in both XRD and Raman spectroscopy, indicating the pure phase of ZnIn<sub>2</sub>S<sub>4</sub> thin films.

More detailed structural information of ZnIn<sub>2</sub>S<sub>4</sub> thin films is revealed via TEM and HRTEM. The TEM image of ZIS-2.5 annealed for 2 h is showed in Fig. 4a, which indicates that the thin films consisted of rod-like ZnIn<sub>2</sub>S<sub>4</sub> nanocrystal. The preferred growth of

the ZnIn<sub>2</sub>S<sub>4</sub> nanocrystal can be observed in TEM image. The width and length of the nanorods are about 13 ± 3 nm and 26 ± 5 nm, respectively. A representative HRTEM image shows clear lattice fringes with interplanar spacings of 0.414 nm for the (006) plane of hexagonal phase ZnIn<sub>2</sub>S<sub>4</sub>, as illustrated in Fig. 4b. The TEM and HRTEM images also indicate the preferred growth along c-axis. Both the grain size and preferred growth of ZnIn<sub>2</sub>S<sub>4</sub> nanocrystal accord with the XRD results.

The cross-sectional and top-view morphology of ZnIn<sub>2</sub>S<sub>4</sub> thin films are investigated by FESEM. The cross-sectional FESEM images of ZIS-2.5 with different annealing times are displayed in Fig. 5a–d. The thin film before annealing looks like amorphous without observation of any grain (Fig. 5a), while nanocrystal small than 10 nm is formed after annealing for 0.5 h (Fig. 5b). However, the growth of grain is not noteworthy with prolonged annealing time, implying the grain is hard to grow through sulfurization in S vapor at 500 °C. It is hard to distinguish the grain boundary of a single nanocrystal due to the denser stacking of nanocrystals, as shown in Fig. 5d. It is similar for the ZIS-2 and ZIS-3 samples annealed for 2 h, while the grain size is a little larger than ZIS-2.5 sample, showed in Fig. 5e and f. As seen in Fig. S1, the top-view morphology of ZIS-2.5 is more and more recognizable with increasing annealing time (Figs. S1a–S1c), the same as cross-sectional morphology. Otherwise, some hexagonal grain can be observed from ZIS-2.5 but not from ZIS-2 and ZIS-3 after annealing for 2 h (Figs. S1d–S1f). All the thin films are smooth and compact without any crack or void.

The optical properties of the ZnIn<sub>2</sub>S<sub>4</sub> thin films are characterized by UV–Vis absorbance spectrums. All ZIS-2.5 samples have a steep absorption edge and the absorption onsets locate around 500 nm, indicating the photoresponse in visible light region (Fig. S2). There is hardly any change of the absorption edge with increasing annealing time. Although the nanocrystal size is very small, no quantum size effect is observed in ZnIn<sub>2</sub>S<sub>4</sub> thin films [8]. On the other hand, the band gap  $E_g$  can be adjusted by controlling the In/Zn ratio in thin films and the absorption edge is red-shifted with increasing In content in ZnIn<sub>2</sub>S<sub>4</sub> thin films, as shown in Fig. 6. The ZnIn<sub>2</sub>S<sub>4</sub> is a direct band gap material, following the formula  $(\alpha h\nu)^2 = A(h\nu - E_g)$ . The plots of the  $(\alpha h\nu)^2$  vs. photon energy ( $h\nu$ ) of ZnIn<sub>2</sub>S<sub>4</sub> are obtained (inset of Fig. 6). Extrapolating this line to the photon energy axis, the band gaps of ZnIn<sub>2</sub>S<sub>4</sub> thin films are estimated to be 2.95, 2.80 and 2.64 eV for ZIS-2, ZIS-2.5 and ZIS-3, respectively.

The electrochemical impedance measurements of ZnIn<sub>2</sub>S<sub>4</sub> thin films are measured in 0.25 M Na<sub>2</sub>S aqueous solution, as shown in Fig. 7a. All the thin films show a positive slope in the Mott–Schottky plots, as expected for n-type semiconductor. The values of flat-band potential in 0.25 M Na<sub>2</sub>S aqueous solution are evaluated to be –1.54, –1.44 and –1.47 V vs. Ag/AgCl electrode for ZIS-2, ZIS-2.5 and ZIS-3 annealed for 2 h, respectively. The flat-band potentials are converted to the normal hydrogen electrode (NHE) by using [24]

$$E(\text{NHE}) = E(\text{Ag/AgCl}) + 0.197 + 0.059 \times \text{pH},$$

and are calculated to be –0.55, –0.45 and –0.48 V vs. NHE for ZIS-2, ZIS-2.5 and ZIS-3, respectively. It is generally believed that the bottom of the conduction band in many n-type semiconductors is more negative by ~0.1 V than the flat-band potential [25]. So the conduction bands can be estimated to be –0.65, –0.55 and –0.58 V vs. NHE for ZIS-2, ZIS-2.5 and ZIS-3, respectively. Because the conduction bands of these samples are more negative than NHE, they are thermodynamically permissible for hydrogen production without any applied voltage. On the other hand, carrier density is inversely proportional to the slope of Mott–Schottky plot [26]. The ZIS-2 shows a smaller slope of Mott–Schottky plot than the other

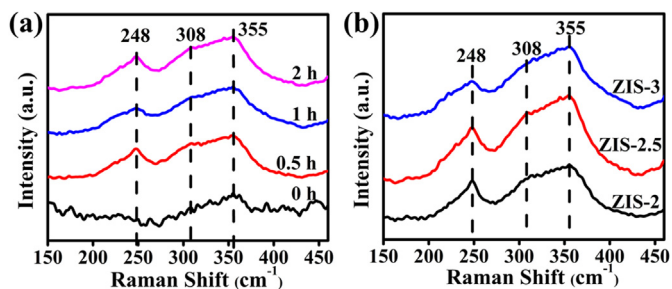


**Fig. 3.** Raman spectra of (a) ZIS-2.5 with different annealing times and (b) ZnIn<sub>2</sub>S<sub>4</sub> thin films with different In/Zn ratios after annealing for 2 h.

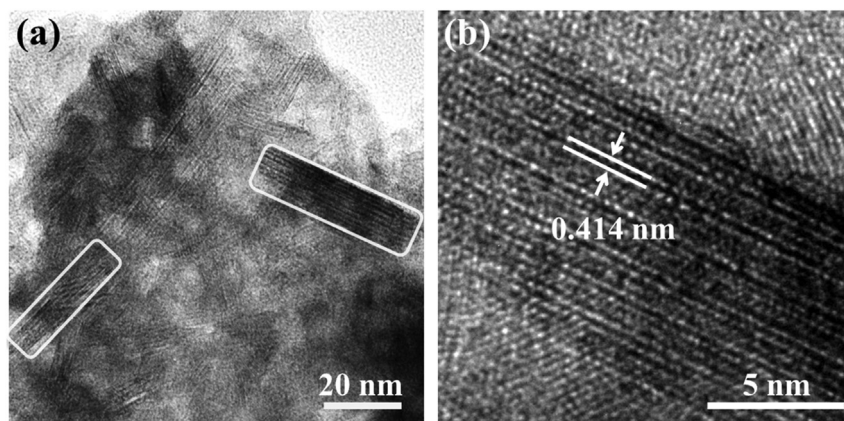


**Fig. 4.** (a) TEM and (b) HRTEM images of rod-like  $\text{ZnIn}_2\text{S}_4$  nanocrystal in ZIS-2.5 annealed for 2 h.

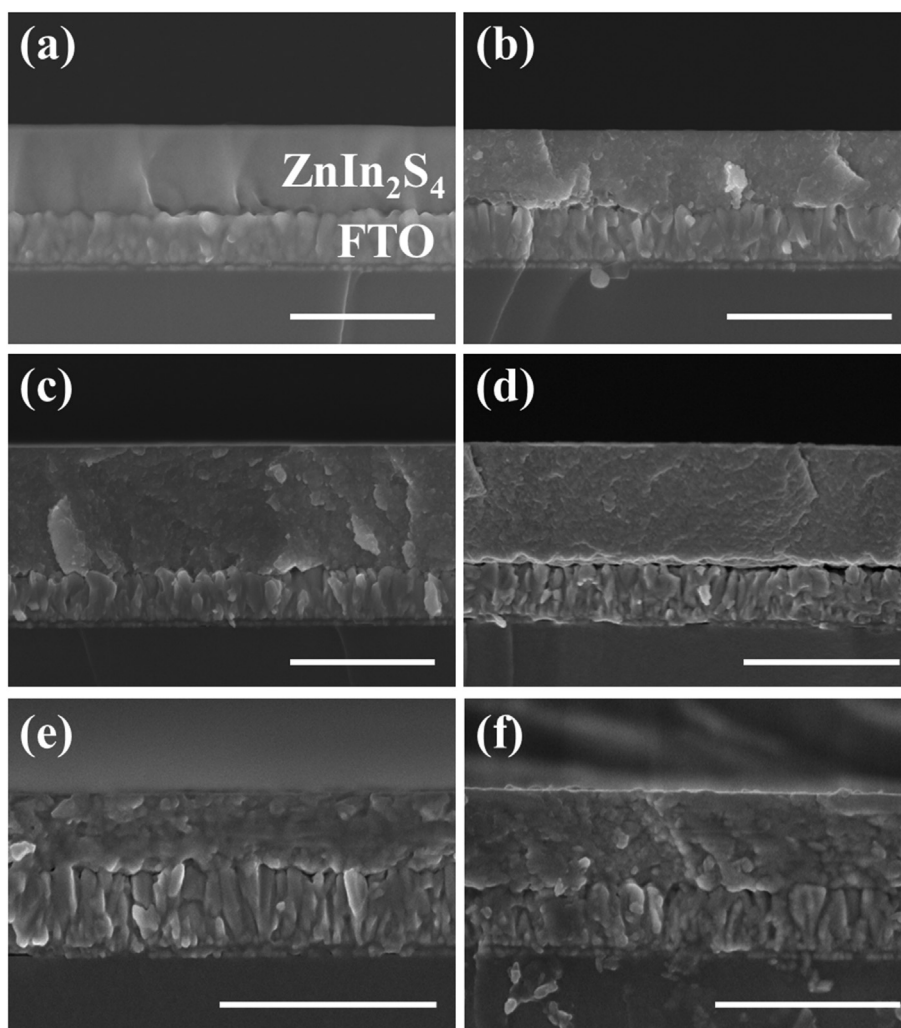


**Fig. 5.** Cross-sectional FESEM images of  $\text{ZnIn}_2\text{S}_4$  thin films with different annealing times and In/Zn ratios (a) ZIS-2.5 annealed for 0 h, (b) ZIS-2.5 annealed for 0.5 h, (c) ZIS-2.5 annealed for 1 h, (d) ZIS-2.5 annealed for 2 h, (e) ZIS-2 annealed for 2 h and (f) ZIS-3 annealed for 2 h (scale bar 1  $\mu\text{m}$ ).

two samples, suggesting the higher carrier density. The slopes of ZIS-2.5 and ZIS-3 are almost the same, meaning that these two samples had similar carrier density.

The performance of the  $\text{ZnIn}_2\text{S}_4$  thin films in solar energy conversion is examined by PEC measurement. Fig. 7b shows the typical

chopped current density ( $J$ ) vs. applied potential ( $E$ ) measurements under visible light illumination (simulated solar light illumination cut off by a 400 nm filter) for all three samples with applied potentials in the range from  $-1.3$  to  $0.6$  V vs. an Ag/AgCl electrode in  $0.25$  M  $\text{Na}_2\text{S}$  aqueous solution. ZIS-3 achieves the highest light

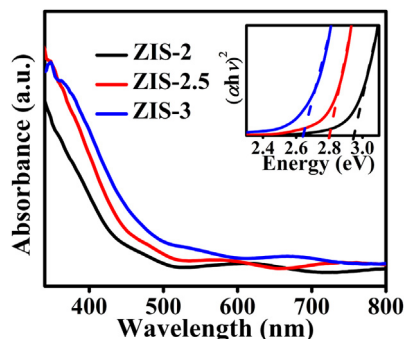


Fig. 6. UV–Vis absorbance spectra of  $\text{ZnIn}_2\text{S}_4$  thin films with different In/Zn ratios after annealing for 2 h. Inset shows the  $E_g$  derived from  $(\alpha h\nu)^2 - h\nu$  curves.

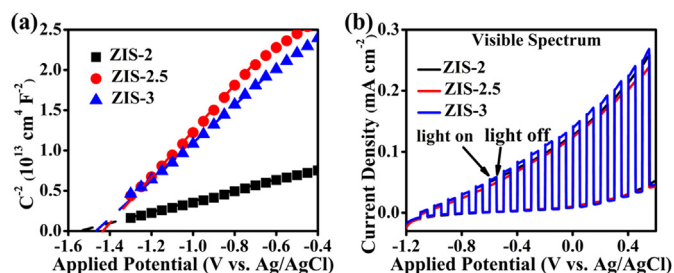


Fig. 7. (a) Mott–Schottky plots of  $\text{ZnIn}_2\text{S}_4$  thin films with different In/Zn ratios collected at a frequency of 5 kHz in the dark. (b) Chopped  $J$ – $V$  curves of  $\text{ZnIn}_2\text{S}_4$  thin films annealed for 2 h with different In/Zn ratios under simulated solar light (AM 1.5) illumination cut off by a 400 nm filter in 0.25 M  $\text{Na}_2\text{S}$  electrolyte.

current density ( $0.27 \text{ mA cm}^{-2}$ ) because of its smallest  $E_g$ , which can utilize more visible light to produce photo-generated carrier. Although the  $E_g$  of ZIS-2.5 is smaller than that of ZIS-2, the higher carrier density of ZIS-2 may contribute to light current as the dominant sector, which results in the slight higher light current density contrast to ZIS-2.5. The result of PEC measurement changes under simulated solar light illumination, as shown in Fig. S3. ZIS-2 gets the highest light current density thanks to the higher carrier density. Given ZIS-2.5 and ZIS-3 have the similar carrier density, the higher light current density of ZIS-3 comparing with that of ZIS-2.5 should be owing to the utilization of more light because of the smaller  $E_g$  of ZIS-3. What's more, the visible light current occupies nearly 60% of the full spectrum light current, indicating the excellent visible light response of the  $\text{ZnIn}_2\text{S}_4$  thin films.

#### 4. Conclusion

Hexagonal phase  $\text{ZnIn}_2\text{S}_4$  nanocrystalline thin films are successfully deposited by a solution method using spin-coating and annealing process. Precursor solution is prepared by dissolution of  $\text{ZnO}$  and  $\text{In}(\text{OH})_3$  in thioacetic acid-based solution, avoiding the introduction of any anion impurity. The In/Zn ratio in  $\text{ZnIn}_2\text{S}_4$  thin film can be effectively adjusted by controlling the metal source components in precursor solution. The hexagonal  $\text{ZnIn}_2\text{S}_4$  with different In/Zn ratios grow along  $c$ -axis after annealing in S vapor at  $500^\circ\text{C}$ , resulting in the formation of rod-like nanocrystal. The grain is difficult to grow with prolonged annealing time, and the width and length of nanocrystal are about  $13 \pm 3 \text{ nm}$  and  $26 \pm 5 \text{ nm}$  after annealing for 2 h. The conduction bands of  $\text{ZnIn}_2\text{S}_4$  thin films derived from Mott–Schottky plots are more negative than NHE, implying they are thermodynamically permissible for hydrogen

production without any applied voltage. ZIS-3 gets the highest light current under visible light illumination owing to the utilization of more visible light because of the smallest  $E_g$  of ZIS-3, while the achievement of highest light current under full spectrum illumination by ZIS-2 should be ascribing to its higher carrier density. The light current under visible light illumination occupies almost 60% of the light current under full spectrum illumination, indicating the excellent visible light response of the  $\text{ZnIn}_2\text{S}_4$  thin films. What's more, many other high-quality thin films of multi metal chalcogenides can be fabricated by this facile solution-based method via solving other metal oxides and hydroxides in the solution.

#### Acknowledgments

This work is financially supported by National 863 Program of China (Grant 2011AA050505), National Natural Science Foundation of China (Grant Nos. 91122034, 51125006, 51121064 and 61204072), and Science and Technology Commission of Shanghai Grant (Nos. 12XD1406800).

#### Appendix A. Supplementary data

Supplementary data related to this article can be found in the online version at <http://dx.doi.org/10.1016/j.jpowsour.2014.03.063>.

#### References

- [1] Z. Lei, W. You, M. Liu, G. Zhou, T. Takata, M. Hara, K. Domen, C. Li, *Chem. Commun.* 17 (2003) 2142–2143.
- [2] N. Romeo, A. Dallaturca, R. Braglia, G. Sberveglieri, *Appl. Phys. Lett.* 22 (1973) 21–22.
- [3] W.S. Seo, R. Otsuka, H. Okuno, M. Ohta, K. Koumoto, *J. Mater. Res.* 14 (1999) 4176–4181.
- [4] Z. Chen, J. Xu, Z. Ren, Y. He, G. Xiao, *J. Solid State Chem.* 205 (2013) 134–141.
- [5] L. Shang, C. Zhou, T. Bian, H. Yu, L.Z. Wu, C.H. Tung, T. Zhang, *J. Mater. Chem. A* 1 (2013) 4552–4558.
- [6] H. Jia, W. He, Y. Lei, X. Chen, Y. Xiang, S. Zhang, W.M. Lau, Z. Zheng, *RSC Adv.* 3 (2013) 8909–8914.
- [7] L. Mandal, N.S. Chaudhari, S. Ogale, *ACS Appl. Mater. Inter.* 5 (2013) 9141–9147.
- [8] S. Peng, L. Li, Y. Wu, L. Jia, L. Tian, M. Srinivasan, S. Ramakrishna, Q. Yan, S.G. Mhaisalkar, *Cryst. Eng. Comm.* 15 (2013) 1922–1930.
- [9] X. Gou, F. Cheng, Y. Shi, L. Zhang, S. Peng, J. Chen, P. Shen, *J. Am. Chem. Soc.* 128 (2006) 7222–7229.
- [10] L. Shi, P. Yin, Y. Dai, *Langmuir* 29 (2013) 12818–12822.
- [11] X. Hu, J.C. Yu, J. Gong, Q. Li, *Cryst. Growth Des.* 7 (2007) 2444–2448.
- [12] Y. Chen, S. Hu, W. Liu, X. Chen, L. Wu, X. Wang, P. Liu, Z. Li, *Dalt. Trans.* 40 (2011) 2607–2613.
- [13] R. Nomura, H. Matsuda, T. Miyai, A. Baba, *Thin Solid Films* 342 (1999) 108–112.
- [14] J. Yin, J. Jia, G. Yi, L. Wang, *J. Chin. Chem. Soc.* 59 (2012) 1365–1368.
- [15] S. Peng, P. Zhu, V. Thavasi, S.G. Mhaisalkar, S. Ramakrishna, *Nanoscale* 3 (2011) 2602–2608.
- [16] K.W. Cheng, C.J. Liang, *Sol. Energ. Mater. Sol. C* 94 (2010) 1137–1145.
- [17] K.W. Cheng, C.M. Huang, Y.C. Yu, C.T. Li, C.K. Shu, W.L. Liu, *Sol. Energ. Mater. Sol. C* 95 (2011) 1940–1948.
- [18] H. Yu, X. Quan, Y. Zhang, N. Ma, S. Chen, H. Zhao, *Langmuir* 24 (2008) 7599–7604.
- [19] L. Vayssieres, K. Keis, S.E. Lindquist, A. Hagfeldt, *J. Phys. Chem. B* 105 (2001) 3350–3352.
- [20] Y. Liu, Y. Xie, H. Cui, W. Zhao, C. Yang, Y. Wang, F. Huang, N. Dai, *Phys. Chem. Chem. Phys.* 15 (2013) 4496–4499.
- [21] Y. Liu, F. Huang, Y. Xie, H. Cui, W. Zhao, C. Yang, N. Dai, *J. Phys. Chem. C* 117 (2013) 10296–10301.
- [22] S. Ahn, T.H. Son, A. Cho, J. Gwak, J.H. Yun, K. Shin, S.K. Ahn, S.H. Park, K. Yoon, *Chem. Sus. Chem.* 5 (2012) 1773–1777.
- [23] S. Shen, P. Guo, L. Zhao, Y. Du, L. Guo, *J. Solid State Chem.* 184 (2011) 2250–2256.
- [24] M.W. Kanan, D.G. Nocera, *Science* 321 (2008) 1072–1075.
- [25] Y. Chen, R. Huang, D. Chen, Y. Wang, W. Liu, X. Li, Z. Li, *ACS Appl. Mater. Inter.* 4 (2012) 2273–2279.
- [26] Z. Wang, C. Yang, T. Lin, H. Yin, P. Chen, D. Wan, F. Xu, F. Huang, J. Lin, X. Xie, *Energy Environ. Sci.* 6 (2013) 3007–3014.